Ultrasonics - Sonochemistry 53 (2019) 11–24

Contents lists available at ScienceDirect

Ultrasonics - Sonochemistry

journal homepage: www.elsevier.com/locate/ultson

Simulation of cavitation enhanced temperature elevation in a soft tissue during high-intensity focused ultrasound thermal therapy

E.M. Zilonova[a], M. Solovchuk[a,d,*], T.W.H. Sheu[a,b,c]

[a] Department of Engineering Science and Ocean Engineering, National Taiwan University, No. 1, Section 4, Roosevelt Road, Taipei 10617, Taiwan, ROC
[b] Center of Advanced Study in Theoretical Science (CASTS), National Taiwan University, Taiwan, ROC
[c] Department of Mathematics, National Taiwan University, Taiwan, ROC
[d] Institute of Biomedical Engineering and Nanomedicine, National Health Research Institutes, No. 35, Keyan Road, Zhunan 35053, Taiwan, ROC

ARTICLE INFO

Keywords:
Cavitation in soft tissue
Temperature distribution
Vapor mass diffusion
High-intensity focused ultrasound
Heat deposition

ABSTRACT

The present study aims to investigate temperature distribution caused by bubble oscillations in a soft tissue during focused ultrasound therapy by introducing a coupled temperature-cavitation model. The proposed model is capable of describing bubble dynamics, viscoelastic properties of surrounding tissue-like medium, temperature distribution inside and outside the bubble, vapor diffusion within the bubble and vapor flux through the bubble wall to the exterior. The continuous temperature distribution inside and outside the oscillating bubble in soft tissue subject to ultrasound wave with high acoustic pressure is presented. The temperature close to the bubble wall can reach the value of about 10^3 K. The elasticity of soft tissue reduces temperature values. The relaxation time effect strongly depends on the period of the ultrasound wave. If the vapor mass flux effect is taken into account in the simulations, the rectified growth effect can be observed, which can lead to the decrease of the temperature values. Due to the growth of the bubble, the effects of elasticity and relaxation time on the temperature become less prominent during several bubble oscillation cycles. The impact of cavitation heat source terms on the exterior temperature was examined and led us to draw conclusion that, even though these heat sources can increase the outside temperature values, they can not be treated as main mechanisms for the temperature elevation during a few microseconds. The performed comparison with uncoupled conventional model for the outside temperature calculation revealed that coupling with inside temperature model delivers incomparably higher values to the bubble's exterior and, therefore, it is essential for the accurate description of the treatment process.

1. Introduction

High negative pressure and high temperature values within the medium can lead to bubble formation, a phenomenon known as acoustic cavitation. Originally, cavitation has been studied for hydrodynamic applications. However, recently its biomedical applications such as biomedical imaging and therapeutic ultrasound have become popular. High intensity focused ultrasound is a rapidly developing medical technology for fully noninvasive surgery. Nowadays, it has a wide range of applications (such as tumor ablation in different parts of the body, acoustic hemostasis, drug and gene delivery, treatment of neurological disorders [1–5]). Our research will be mainly focused on the tumor ablation procedure, even though the results of the study can be applied to a wide variety of problems. The tumor ablation procedure (Fig. 1) is a result of the conversion of focused ultrasound energy into thermal energy that is able to quickly elevate the tissue temperature, which, in turn, results in an occurrence of the thermal coagulation necrosis (with the temperature higher than 55 °C). Coagulation necrosis leads to tumor cells' destruction. Cavitation presence can enhance heat deposition and is able to significantly increase the tissue temperature. Also, the presence of cavitation effect makes the prediction of the treatment process more complicated [6,7]. Cavitation can also enhance drug delivery and assist drug uptake by cells. Nowadays, it is still not clear, which cavitation effects: thermal or mechanical (microstreaming, shear stresses, mechanical forces, microjets) play the key role in therapeutic applications of ultrasound. In this paper, we will focus on thermal effects associated with a cavitation presence in soft tissue. Tissue heating can be well described by bioheat equation [7–9]. Nevertheless, when cavitation takes place, the bioheat equation in its original form can not describe the heating process precisely any longer.

* Corresponding author at: Institute of Biomedical Engineering and Nanomedicine, National Health Research Institutes, No. 35, Keyan Road, Zhunan 35053, Taiwan, ROC.
E-mail addresses: zilorina@mail.ru (E.M. Zilonova), solovchuk@gmail.com (M. Solovchuk), twhsheu@ntu.edu.tw (T.W.H. Sheu).

https://doi.org/10.1016/j.ultsonch.2018.12.006
Received 20 April 2018; Received in revised form 5 December 2018; Accepted 5 December 2018
Available online 05 December 2018
1350-4177/

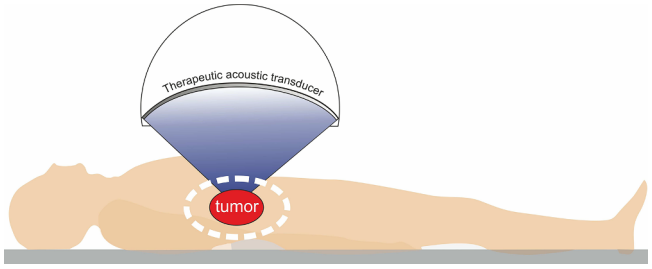

Fig. 1. Schematic of the tumor ablation procedure in HIFU thermal therapy.

Therefore, the conventional theory should be refined in order to take into account tissue heating due to the bubble's presence. The present study is going to be focused on the investigation of the temperature elevation inside and outside the bubble in a soft tissue exposed to HIFU pulse application. This temperature distribution is essential for a better and more profound understanding of cavitation impact on the tumor ablation process and other therapeutic modalities.

Temperature distribution associated with bubble oscillations has been a subject of interest for many authors. The early studies investigated the temperature within the bubble [10–17]. For this purpose, different approaches have been applied. However, they all focused on the inside temperature calculation, whereas the outside temperature was assumed to be unperturbed. Later studies started to investigate the cavitation enhanced heating in the surrounding medium [18–23]. The main approach here was an addition of extra heat sources responsible for the bubble presence into the heat equation for the outside medium. However, the major disadvantage of this approach was that the temperatures inside and outside the bubble were still not interrelated. Coupling of the inside and outside temperatures of the bubble was made by Stricker et al. [24] and Kamath et al. [25]. Shpak et al. [26] extended this coupling approach by considering the vapor flux through the bubble wall. Nevertheless, Kamath et al. [25], Stricker et al. [24], Shpak et al. [26] all considered water as a surrounding medium. Therefore, this study has been refined further by consideration of tissue-like surrounding medium by Barajas and Johnsen [27].

Our objective is to develop a new accurate model for the simulation of bubble dynamics in soft tissue and the corresponding temperature distribution during HIFU thermal therapy. In order to describe precisely the thermal behavior associated with bubble oscillations, the temperature should be continuous in space; hence, both temperatures inside and outside the bubble should be interrelated. The applicability of the proposed model to a high acoustic pressure that occurs during HIFU therapy is obtained by the employment of Gilmore-Akulichev cavitation model for the simulation of bubble dynamics. Gilmore-Akulichev model [28] can deal with the case of high Mach number that takes place during bubble collapse. The frequently used Keller-Miksis cavitation model [24–27] is suitable for the description of bubble oscillations under moderate amplitudes and frequencies of the driving pulse that correspond to a sufficiently low Mach number. However, the authors deem the Keller-Miksis model not to be the best choice for a high acoustic pressure that occurs during HIFU therapy. As we showed in [29], Keller-Miksis model can exceed its applicability range of Mach number smaller than $\left(\frac{\dot{R}}{c_\infty} < 1\right)$ during bubble collapse. Also, the majority of studies consider water as a surrounding medium [24–26], so the Newtonian model for the stress calculation was employed in their research. Whereas for our study, Zener viscoelastic model would be employed in order to simulate some important soft tissue features such as elasticity and relaxation time [30].

In the current paper, temperature elevation associated with cavitation in soft tissue is modeled by two coupled heat equations for the temperature inside and outside the bubble. For the inside temperature simulation, the commonly used model of Prosperetti [15] is employed. Temperature elevation in tissue can be described by multiple bioheat models: Pennes model [31], Wulff model [32], Chen and Holmes model [33], porous media model [34,35] and other models. Due to the bubble's micron size, oscillations are assumed to take place in interstitial fluid that bathes tissue cells (rather than in a vascular system). Hence, bioheat equation [32] that incorporates the direct convection term caused by the interstitial fluid is applied in the bubble's exterior.

Following the approach of [36,27,26], energy equation for the bubble's interior is refined in order to take into account vapor diffusion and its mass transfer across the bubble surface (bubble is considered to be a mixture of non-condensible gas and vapor).

The current study proposes a new coupled model that incorporates bubble dynamics model, a viscoelastic model for soft tissue simulation, two temperature models for bubble's interior and exterior and diffusion model for the calculation of vapor mass concentration within the bubble. It is suitable for the prediction of the temperatures inside and outside the bubble when it oscillates in soft tissue during HIFU therapy. The continuous temperature distribution inside and outside the oscillating bubble with high acoustic pressure is presented. Even consideration of the convective cooling from the interstitial fluid still leads to an abnormally high temperature outside the bubble. The inclusion of cavitation heat sources into the bubble's exterior is studied in order to reveal if we have a necessity to take them into account. Temperature's sensitivity with respect to the soft tissue properties and vapor mass transfer is examined. At high ultrasound powers, vapor mass transfer is found to impact temperature distribution. The present paper also compares the proposed model with the uncoupled conventional temperature models.

2. Formulation

2.1. Gilmore-Akulichev-Zener model

As a cavitation model for the modeling of bubble dynamics in soft tissue, we employ Gilmore-Akulichev-Zener model [29]. The model is written as follows:

$$R\ddot{R}\left(1-\frac{\dot{R}}{C_l}\right)+\frac{3}{2}\dot{R}^2\left(1-\frac{\dot{R}}{3C_l}\right)=\left(1+\frac{\dot{R}}{C_l}\right)\times\left(H-\frac{\tau_{rr}|_R}{\rho_t}+\frac{3q}{\rho_t}\right)-\frac{R}{C_l}\left[\dot{H}\left(1-\frac{\dot{R}}{C_l}\right)-\frac{1}{\rho_t}\frac{d}{dt}\tau_{rr}|_R+\frac{1}{\rho_t}\frac{d}{dt}(3q)\right], \tag{1}$$

$$H=\frac{1}{\rho_t}\frac{n}{n-1}(p_0+p(t)+B)\times\left\{\left[\frac{\left(p_{in}-\frac{2S}{R}+\tau_{rr}|_R\right)+B}{p_0+p(t)+B}\right]^{\frac{n-1}{n}}-1\right\}, \tag{2}$$

$$C_l=c_\infty\left[\frac{\left(p_{in}-\frac{2S}{R}+\tau_{rr}|_R\right)+B}{p_0+p(t)+B}\right]^{\frac{n-1}{2n}}, \tag{3}$$

$$q+\lambda\dot{q}+\lambda\frac{\dot{R}\tau_{rr}|_R}{R}=\frac{1}{3}\left[-\frac{4G}{3R^3}(R^3-R_0^3)-4\mu\frac{\dot{R}}{R}\right], \tag{4}$$

$$\tau_{rr}|_R+\lambda\dot{\tau}_{rr}|_R=-\frac{4G}{3}\left(1-\frac{R_0^3}{R^3}\right)-4\mu\frac{\dot{R}}{R}. \tag{5}$$

In the above equations, $R(t)$ is the radius of the bubble, r the distance from the center of bubble, H an enthalpy, C_l the local sound speed at the

bubble wall, c_∞ the speed of sound, ρ_t the tissue density, τ_{rr} the stress in a motion in r direction, B and n the particular liquid constants (that were set for tissue accordingly to [20]), p_0 the static background pressure, $p(t)$ the varying driving sound field, p_{in} the pressure inside the bubble, S the surface tension, λ the tissue relaxation time, G the tissue elasticity, μ the tissue viscosity, R_0 the initial bubble radius. Variable q is equal to $q = \int_R^\infty \frac{\tau_{rr}(r,t)}{r} dr$ and it was introduced in order to couple the cavitation model with the Zener viscoelastic model [29,30].

2.2. Temperature inside the bubble

For the simulation of temperature inside the bubble, the model proposed by [15,16] is used. This model consists of solving the energy equation inside the bubble. The inside temperature is a function of time and distance measured from the center of the bubble that makes the temperature distribution more realistic:

$$\frac{\gamma}{\gamma-1}\frac{p_{in}}{T_{in}}\frac{\partial T_{in}}{\partial t} = -\frac{\gamma}{\gamma-1}\frac{p_{in}}{T_{in}}U\frac{\partial T_{in}}{\partial r} + \frac{dp_{in}}{dt} + \nabla_r\cdot(K_g\nabla_r T_{in}), \tag{6}$$

$$U = \frac{1}{\gamma p_{in}}\left[(\gamma-1)K_g\frac{\partial T_{in}}{\partial r} - \frac{r}{3}\frac{dp_{in}}{dt}\right], \tag{7}$$

$$\frac{dp_{in}}{dt} = \frac{3}{R}\left[-\gamma p_{in}\dot{R} + (\gamma-1)K_g\left|_R\frac{\partial T_{in}}{\partial r}\right|_R\right], \tag{8}$$

where $T_{in}(r, t)$ is the temperature inside the bubble, $\gamma = 1.4$ the specific heats ratio, K_g the thermal conductivity of gas (or some mixture inside the bubble). Following [15], K_g can be approximated as a linear function of T_{in}: $K_g = A_g T_{in} + B_g$, where $A_g = 5.3 * 10^{-5}$ W/(m·K^2), $B_g = 1.17 * 10^{-2}$ W/(m·K) are the numerical values.

2.3. Temperature inside the bubble with vapor mass transfer

With the assumption that the bubble is a mixture of non-condensible gas and water vapor, the equation corresponding to the diffusion inside the bubble is added in a form of Fick's law with respect to the vapor mass concentration C [36,27]. The inside bubble pressure p_{in} is assumed to follow the perfect gas law, where the effective gas constant is given by a mass-weighted average of each of the components $\Re = C\Re_v + (1-C)\Re_g$, where $\Re_v$ is the perfect vapor constant and is the perfect gas constant. The term corresponding to the vapor mass transfer $\dot{m}_v''$ across the bubble wall was obtained from the equation accounting for the conservation of energy and can be found in [36]. With the above-mentioned assumptions, the temperature, pressure, and vapor mass concentration within the bubble can be described by the following equations:

$$\frac{\gamma}{\gamma-1}\frac{p_{in}}{T_{in}}\frac{\partial T_{in}}{\partial t} = -\frac{\gamma}{\gamma-1}\frac{p_{in}}{T_{in}}U\frac{\partial T_{in}}{\partial r} + \frac{dp_{in}}{dt} + \nabla_r\cdot\left(K_g\nabla_r T_{in}\right), \tag{9}$$

$$U = \frac{1}{\gamma p_{in}}\left[(\gamma-1)K_g\frac{\partial T_{in}}{\partial r} - \frac{r}{3}\frac{dp_{in}}{dt}\right], \tag{10}$$

$$\frac{dp_{in}}{dt} = \frac{3}{R}\left[-\gamma p_{in}\dot{R} + (\gamma-1)K_g\left|_R\frac{\partial T_{in}}{\partial r}\right|_R + \gamma\Re_v\dot{m}_v''T_{in}\right|_R\Bigg], \tag{11}$$

$$\frac{\partial C}{\partial t} + u\frac{\partial C}{\partial r} = D\frac{\nabla_r\cdot(\rho_m\nabla_r C)}{\rho_m}, \tag{12}$$

$$u = U + D\frac{\Re_v - \Re_g}{C\Re_v + (1-C)\Re_g}\frac{\partial C}{\partial r},$$
$$\rho_m = \frac{p_{in}}{[C\Re_v + (1-C)\Re_g]T_{in}}, \tag{13}$$

$$\dot{m}_v'' = D\frac{\rho_m|_R}{1-C|_R}\frac{\partial C}{\partial r}\Bigg|_R, \tag{14}$$

where $C = \frac{\rho_v}{\rho_m}$ is the vapor mass concentration, ρ_v the vapor density, ρ_m the gas–vapor mixture density, $\dot{m}_v''$ the vapor flux across the interface and D the diffusion coefficient.

2.4. Temperature in tissue outside the bubble

For the calculation of the temperature outside the bubble, the bioheat equation is used in the form proposed by Wulff [32] with a direct convention term. The size of the cavitation bubble during different oscillation phases in the thermal therapy is known to be in a range from 10^{-8} m to 10^{-5} m [6,21,37]. The majority of the eukaryotic human cells found in soft tissues take the order of 10^{-6} m–10^{-5} m [38]. Hence, the size of the cavitation bubble is comparable to the tissue cells size. Tissue cells reside in highly specialized structures – extracellular matrices (ECM) that represent interlocking mesh around cells and consist of a mixture of protein molecules [39,40]. The immediate environment that surrounds each individual cell in the body is the extracellular fluid. 75–80 percent of the extracellular fluid is an interstitial fluid that lies around and between cells and fills extracellular matrices spaces [41]. In a bubble scale that is of the order of a micron, this interstitial fluid can be responsible for the heat convection. The velocity of the surrounding medium in the convection term is approximated from the continuity equation [24,42]. With the addition of the extra cavitation heat sources [6], the bioheat equation for soft tissue is used in the following form:

$$\rho_t c_t\frac{\partial T_{out}}{\partial t} = \nabla\cdot(K_t\nabla T_{out}) - \left(\rho_I c_I\frac{R^2\dot{R}}{r^2}\right)\cdot\nabla T_{out} + q_{ac} + q_{visc} + q_{rad}, \tag{15}$$

where T_{out} is the temperature outside the bubble, c_t the specific heat and K_t the tissue thermal conductivity, ρ_I the interstitial fluid density and c_I the interstitial fluid specific heat. The second term on the right-hand side of the above equation accounts for the discussed convection caused by the interstitial fluid.

The interstitial fluid has a different composition in different tissues and depends on the area of the body. Experimental determination of its parameters is challenging. The continuous exchange of oxygen, nutrition, and waste through capillaries walls between blood plasma and interstitial fluid leads to their identity, except for protein concentration [41,43,39]. Therefore, it is a common practice to simulate interstitial fluid as blood plasma (the fluid part of the blood that can pass through capillaries walls), since their structure is similar and blood plasma parameters are widely available [44].

The ultrasound power deposition term q_{ac} is $q_{ac} = \frac{\alpha p(t)^2}{\rho_t c_\infty}$ [45,46], where $p(t)$ is the driving pulse and α is the local acoustic absorption coefficient. The remaining terms q_{visc} and q_{rad} are cavitation terms responsible for viscous damping and absorption of the radiated pressure wave, respectively.

The viscous cavitation energy results from the viscous friction forces and appears at the bubble surface. The viscous damping term is defined as follows:

$$q_{visc} = \begin{cases}\frac{16\pi\mu R\dot{R}^2}{\frac{4}{3}\pi r_{visc}^3}, & r \leqslant r_{visc},\\ 0, & r > r_{visc},\end{cases} \tag{16}$$

where r_{visc} is the radius of the tissue volume, upon which the viscous cavitation energy is distributed. Since viscous energy emission takes place at the bubble surface, r_{visc} should be set close to the bubble surface. Thus, viscous damping term appears only close to the bubble surface.

When the bubble collapses, the acoustic pulse is emitted. The radiated power deposited inside the sphere with radius r_{rad}, where acoustic emission is absorbed, is defined as follows [18]:

$$D_{rad}^{abs} = 4\pi\frac{\rho_t R^2(2\dot{R}^2 + R\ddot{R})^2}{c_\infty}(1 - e^{-2\alpha r_{rad}}). \tag{17}$$

In the above equation, α is the absorption coefficient. Viscous damping energy is distributed close to the bubble surface, whereas the radiated pressure wave, on the contrary, propagates deeply into tissue and is absorbed by the medium. Therefore, r_{rad} should represent a larger volume than r_{visc}. The term that corresponds to the radiated pressure wave caused by bubble collapse is defined as follows [18]:

$$q_{rad} = \begin{cases} \frac{3}{4\pi r_{rad}^3} D_{rad}^{abs}, & r \leqslant r_{rad}, \\ 0, & r > r_{rad}. \end{cases} \tag{18}$$

2.5. Acoustic model

Modeling of acoustic wave propagation in a tissue can be performed using the nonlinear Westervelt equation:

$$\nabla^2 p - \frac{1}{c_\infty^2}\frac{\partial^2 p}{\partial t^2} + \frac{\delta}{c_\infty^4}\frac{\partial^3 p}{\partial t^3} + \frac{\beta}{\rho_t c_\infty^4}\frac{\partial^2 p}{\partial t^2} = 0, \tag{19}$$

where p is the sound pressure, δ is the diffusivity of sound, β is the coefficient of nonlinearity. The above equation takes into account the effects of diffraction, absorption, and nonlinear propagation. In the present paper, for the clarity sake, only linear propagation effect will be considered and the Eq. (19) can be written in a form:

$$\nabla^2 p - \frac{1}{c_\infty^2}\frac{\partial^2 p}{\partial t^2} + \frac{\delta}{c_\infty^4}\frac{\partial^3 p}{\partial t^3} = 0. \tag{20}$$

In this case, pressure has a harmonic form $p = A\sin(2\pi f t)$. Effects of relaxation and nonlinear propagation, including shock waves [47], can be easily taken into account, as it has been done in our previous papers [2,46].

3. Coupled model

Temperature Eqs. (9)–(15) are solved together with the Gilmore-Akulichev-Zener model Eqs. (1)–(5). Both temperature equations are written following the assumption of spherical symmetry. The space axis r is divided into two parts by the bubble wall $r = R(t)$. When $r < R(t)$, inside temperature equation is used, and when $r > R(t)$ outside temperature equation is employed (Fig. 2). For the heat deposition sources that are included in the outside temperature equation, space axis r is also divided into parts. Viscous damping energy is known to act at the bubble surface, therefore, the radius of its impact sphere r_{visc} is set close to the bubble interface $R(t)$. For the radiated pressure source, its radius of impact sphere r_{rad} represents larger volume.

The boundary conditions prescribed at the center of the bubble are $\frac{\partial T_{in}}{\partial r}|_{r=0} = 0$, $\frac{\partial C}{\partial r}|_{r=0} = 0$. The boundary condition for tissue is $T_{out}|_{r=r_{max}} = 37$ °C. At the bubble interface, vapor mass flux condition between interior and exterior is used:

$$L_h \dot{m}_v'' = K_t \left.\frac{\partial T_{out}}{\partial r}\right|_R - K_g \left.\frac{\partial T_{in}}{\partial r}\right|_R, \tag{21}$$

where L_h is the latent heat associated with the phase change at the interface (condensation or evaporation [27]).

Also, the equality of the inside and outside temperatures at the bubble wall is employed: $T_{in}|_{r=R(t)} = T_{out}|_{r=R(t)}$. Therefore, two temperature equations are interrelated. Whereas, the equation for inside temperature is coupled with cavitation model through the pressure inside the bubble p_{in} in Eq. (11).

The boundary condition at the bubble wall for the vapor concentration is [36]:

$$C_{r=R(t)} = \frac{p_{ref}\, e^{-\frac{T_{ref}}{T_{r=R(t)}}}}{p_{gas}\frac{R_v}{R_g} - p_{ref}\, e^{-\frac{T_{ref}}{T_{r=R(t)}}}\left(\frac{R_v}{R_g} - 1\right)}, \tag{22}$$

where $p_{ref}\, e^{-\frac{T_{ref}}{T_{r=R(t)}}}$ denotes the saturated vapor pressure at the bubble wall [36,48]. The above boundary condition arises from the assumption of phase equilibrium at the bubble wall [36].

Initial conditions for the system Eqs. (1)–(5), Eqs. (9)–(15) are given below (if not specified otherwise):

$$\begin{aligned} &R_0 = 1 * 10^{-6}\ \text{m}, \quad \dot{R}_0 = 0, \quad q_0 = 0\ \text{Pa}, \\ &\tau_{rr}^0 = 0\ \text{Pa}, \quad T_{in} = 37\ °\text{C}, \\ &C_0 = 10^{-2}, \quad T_{out} = 37\ °\text{C}. \end{aligned} \tag{23}$$

In our simulations parameters were set according to Table 1.

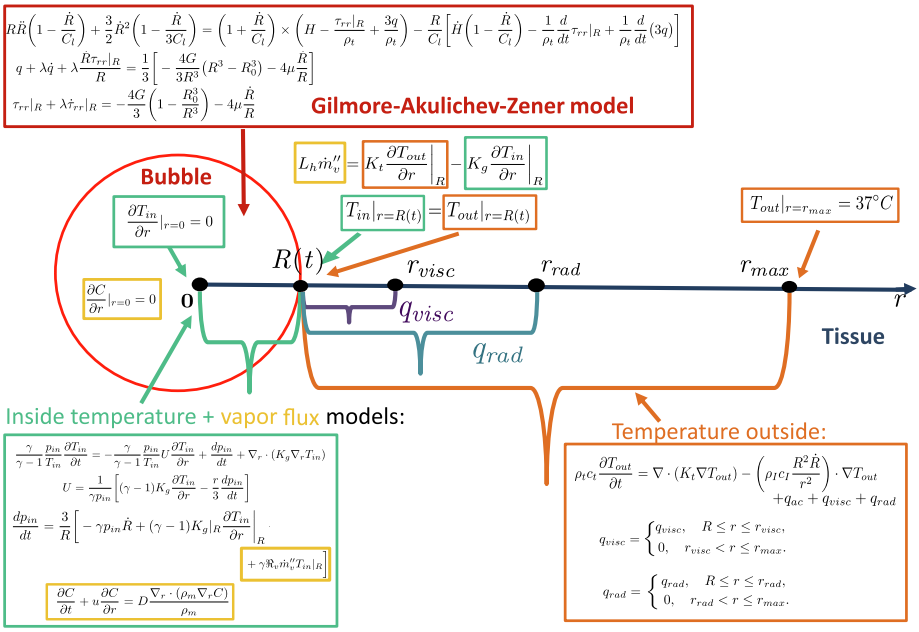

Fig. 2. Schematic of the Gilmore-Akulichev-Zener model coupled with two temperature models (for bubble's interior and exterior, respectively) and diffusion model for vapor mass concentration within the bubble.

Table 1
Simulation parameters.

Nomenclature	Definition	Value	Source
ρ_t	Tissue density	1060 kg/m^3	[45,44]
f	Ultrasound frequency	10^6 Hz	[7]
p_0	Static background pressure	$1.013{\cdot}10^5$ Pa	[42]
S	Surface tension	0.056 kg/s^2	[42,53]
c_∞	Speed of sound	1540 m/s	[42,53]
G	Tissue elasticity	10^6 Pa	[51,52,42,30]
λ	Tissue relaxation time	$3{\cdot}10^{-9}$ s	[30,54]
μ	Tissue viscosity	0.015 Pa·s	[23]
n	Constant in GAZ model	7	[20]
B	Constant in GAZ model	$c_\infty^2\rho_t/n - p_0$	[20]
γ	Specific heat ratio for the bubble's interior	1.4	[15]
$\Re_g$	Perfect gas constant	286.9 m^2/(s^2·K)	[36,55]
$\Re_v$	Perfect vapor constant	461.5 m^2/(s^2·K)	[36,55]
D	Diffusion coefficient	$24.2{\cdot}10^{-6}$ m^2/s	[27]
c_t	Tissue specific heat	3600 J/(kg·K)	[45,44]
K_t	Tissue thermal conductivity	0.512 W/(m·K)	[45,44]
α	Local acoustic absorption coefficient	9 Np/m	[45]
p_{ref}	Empirical parameter for the pressure of the saturated vapor	$1.17 * 10^{11}$ Pa	[36]
T_{ref}	Empirical parameter for the pressure of the saturated vapor	5200 K	[36]
L_h	Latent heat associated with the phase change	$2.264 * 10^6$ J/kg	[27]
c_{IF}	Interstitial fluid specific heat (for blood plasma)	3930 J/ (kg·K)	[44]
ρ_{IF}	Interstitial fluid density (for blood plasma)	1025 kg/m^3	[44]

4. Numerical mesh simplifications

During bubble oscillations, the bubble wall $R(t)$ appears to be in a continuous movement. At the same time, $R(t)$ is the boundary for both spatial domains of temperature equations (the right boundary for the temperature inside the bubble, and the left boundary for the temperature outside the bubble). In order to eradicate the moving numerical mesh, and thereby make the numerical solution more stable, new spatial variables have to be introduced for both temperature equations.

For the temperature equations inside the bubble, the following variables were introduced: $y = \frac{r}{R(t)}$, $r \in [0, R(t)]$ and $\tau = \int_{T_{out}}^{T} K(\theta)d\theta$ [15]. Thus, the moving domain $[0, R(t)]$ was switched to the constant domain $[0, 1]$, such that the numerical mesh also can be defined to be constant. By virtue of the new variables, the system of (9)–(14) is rewritten as follows:

$$\frac{\gamma}{\gamma-1}\frac{p_{in}}{T_{in}K_g}\frac{\partial\tau}{\partial t} = \frac{\gamma}{\gamma-1}\frac{p_{in}}{T_{in}K_g}\times\left(\frac{y\dot{R}}{R}-\frac{U}{R}\right)\frac{\partial\tau}{\partial y} + \frac{dp_{in}}{dt} + \frac{1}{R^2}(\nabla_y^2\tau), \tag{24}$$

$$U = \frac{1}{\gamma p_{in}}\left[(\gamma-1)\frac{1}{R}\frac{\partial\tau}{\partial y} - \frac{yR}{3}\frac{dp_{in}}{dt}\right], \tag{25}$$

$$\frac{dp_{in}}{dt} = \frac{3}{R}\left[-\gamma p_{in}\dot{R} + \frac{\gamma-1}{R}\frac{\partial\tau}{\partial y}\bigg|_{y=1} + \gamma R_v\dot{m}_v''T_{in}(\tau)\bigg|_{y=1}\right], \tag{26}$$

$$\frac{\partial C}{\partial t} = \frac{y\dot{R}-u}{R}\frac{\partial C}{\partial y} + \frac{D}{R^2\rho_m}\left[\nabla_y\cdot\left(\rho_m\nabla_y C\right)\right], \tag{27}$$

$$u = U + D\frac{R_v-R_g}{R[CR_v+(1-C)R_g]}\frac{\partial C}{\partial y},$$
$$\rho_m = \frac{p_{in}}{[CR_v+(1-C)R_g]T_{in}(\tau)}, \tag{28}$$

$$\dot{m}_v'' = D\frac{\rho_m|_{y=1}}{1-C|_{y=1}}\frac{1}{R}\frac{\partial C}{\partial y}\bigg|_{y=1}. \tag{29}$$

According to [15], the temperature dependence of the gas (mixture) thermal conductivity was approximated to be a linear relation $K_g = AT_{in} + B$ and the relation between T_{in} and τ is $T_{in}(\tau) = \frac{[K^2(T_{in}^{\infty})+2A\tau]^{\frac{1}{2}}-B}{A}$.

For the outside temperature, the following spatial variable was introduced $x = \frac{2L}{L+y-1} - 1$, where $y = \frac{r}{R(t)}$, $r \in [R(t), \infty)$ and L is a measure of the thermal diffusion length in tissue, $L = l[\sqrt{K_t/(\rho c_t 2\pi f)}]/R_0$, where f is a frequency of the driving pulse and l is a numerical constant, $l = 20$ [24,27]. Hence, the moving domain outside the bubble $[R(t), \infty)$ was switched to the constant domain $[1, -1)$, thus making the numerical mesh to be constant as well. Eq. (15) is rewritten as follows:

$$\frac{\partial T_{out}}{\partial t} = \frac{(x+1)^3}{LR}\frac{\partial T_{out}}{\partial x}\left\{\frac{K_t}{\rho c_t}\frac{1}{R}\left[\frac{1}{2L} - \frac{1}{L+1+x(1-L)}\right] + \frac{\dot{R}}{2}\frac{\rho_l c_l}{\rho_t c_t}\frac{x+1}{[L+1+x(1-L)]^2} - \frac{\dot{R}}{2}\frac{L+1+x(1-L)}{(x+1)^2}\right\} + \frac{K_t}{\rho_t c_t}\frac{(x+1)^4}{4L^2}\frac{1}{R^2}\frac{\partial^2 T_{out}}{\partial x^2} + \frac{q_{ac}+q_{visc}+q_{rad}}{\rho_t c_t}, \tag{30}$$

$$q_{visc} = \begin{cases} \frac{16\pi\mu R\dot{R}^2}{\frac{4}{3}\pi R^3\left(1-L+\frac{2L}{x_{visc}+1}\right)^3}, & x \geqslant x_{visc}, \\ 0, & x < x_{visc}, \end{cases} \tag{31}$$

$$q_{rad} = \begin{cases} \frac{3}{4\pi R^3\left(1-L+\frac{2L}{x_{rad}+1}\right)^3}D_{rad}^{abs}\left[R\left(1-L+\frac{2L}{x_{rad}+1}\right)\right], & x \geqslant x_{rad}, \\ 0, & x < x_{rad}. \end{cases} \tag{32}$$

The boundary condition at the bubble surface, given in Eq. (21), in the new coordinate system is rewritten as following:

$$\frac{K_t}{R}\frac{(x+1)^2}{2L}\frac{\partial T_{out}}{\partial x}\bigg|_{x=1} + \frac{1}{R}\frac{\partial\tau}{\partial y}\bigg|_{y=1} = -L\dot{m}_v''(y). \tag{33}$$

5. Verification

In our previous paper, bubble dynamics model has been validated by comparing the numerical solution with analytical and numerical results of other authors [29]. The verification of the current model and numerical solution for the temperature was performed through the comparison with the case presented in [24]. The case consists of simulation of a large bubble collapse ($R_0 = 220 * 10^{-6}$ m) with quite a low driving pulse amplitude and frequency ($A = 70 * 10^3$ Pa, $f = 20 * 10^3$ Hz). The temperature distributions obtained by the current model can be found in Fig. 3. It can be seen that current results have a very good agreement with those in [24]. Even though the cavitation models are different, we employ Gilmore-Akulichev-Zener model, whereas in [24] Keller-Miskis equation was used with Newton model for viscosity, solutions coincide because of the choice of parameters. Elasticity G and relaxation time λ in Zener model are set to zero, thus simplifying it to the basic Newton model. Also, in [29], we showed that simulated results from Gilmore-Akulichev-Zener model show good agreement with those obtained from the Keller-Miksis-Zener model at low amplitudes of the driving pulse. Authors of [24] considered bubble oscillations in liquid. Therefore, the energy Eq. (15) for the temperature outside the bubble contains a convection term. The omission of this term results in a significant increase of the outside temperature close to the bubble wall, as shown in Fig. 4. Hence, the convection term in the energy equation is crucial to the temperature distribution. Furthermore,

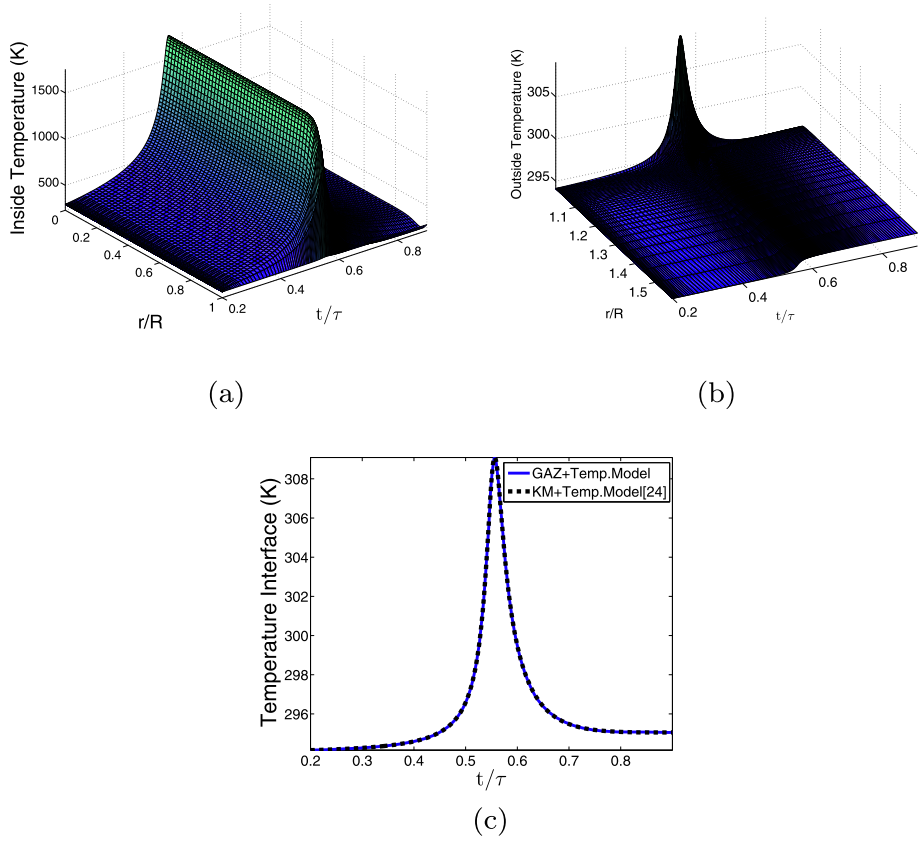

Fig. 3. Verification of the current model by comparing with the results presented in [24], r is the distance from the center of the bubble, $R(t)$ is the bubble radius, τ is the period of the driving pulse. a) Spatial and temporal distributions of the temperature inside the bubble. b) Spatial and temporal distributions of the temperature outside the bubble. c) Tissue temperature at the bubble wall. $p(t) = A\cos(2\pi ft)$, $A = 70 * 10^3$ Pa, $f = 20 * 10^3$ Hz, $R_0 = 220 * 10^{-6}$ m, $c_\infty = 1481$ m/s, $\rho = 1000$ kg/m^3, $\sigma = 0.072$ kg/s^2, $\mu = 0.001$ Pa·s, $G = 0$ Pa, $\lambda_1 = 0$ s, $c_t = 4182$ J/(kg·K), $K = 0.59$ W/(m·K), $T_{in}(0, r) = T_{out}(0, r) = 293.15$ K.

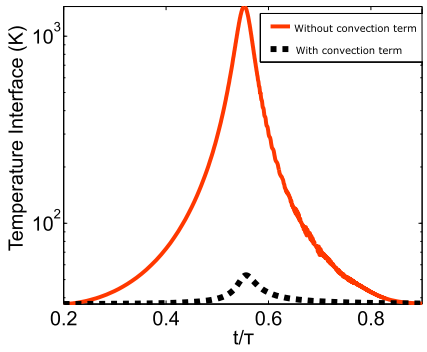

Fig. 4. The comparison of the predicted tissue temperatures at the bubble wall with and without consideration of the convection term. r – distance from the center of the bubble, τ is the period of the driving pulse. $p(t) = A\cos(2\pi ft)$, $A = 70 * 10^3$ Pa, $f = 20 * 10^3$ Hz, $R_0 = 220 * 10^{-6}$ m, $c_\infty = 1481$ m/s, $\rho = 1000$ kg/m^3, $\sigma = 0.072$ kg/s^2, $\mu = 0.001$ Pa·s, $G = 0$ Pa, $\lambda_1 = 0$ s, $c_t = 4182$ J/(kg·K), $K = 0.59$ W/(m·K), $T_{in}(0, r) = T_{out}(0, r) = 293.15$ K.

in this paper we are going to include a convection term in our bioheat equation for the outside temperature, in as much as we are modeling the convection caused by the interstitial fluid of soft tissue, as it was described above. It is worth to mention that the convection term should be omitted if the surrounding medium does not incorporate any fluid part.

6. Results

Due to the recent emergence of different biomedical applications of ultrasound, including HIFU and contrast agents, there is a growing interest in understanding the bubble dynamics in the viscoelastic medium. For the safety and efficiency of different biomedical applications, it is necessary to fathom the temperature distribution both inside the cavitation bubble and in the surrounding tissue. Two coupled heat equations inside and outside the bubble will be solved simultaneously in viscoelastic medium with the temperature being continuous across the bubble interface.

In the current section, the temperature trends inside and outside the oscillating bubble will be examined with respect to the different viscoelastic properties of soft tissue. The contribution of vapor mass flux through the bubble wall to the temperature dynamics will be investigated. The importance of taking into account the thermal energy rising from viscous friction forces at the bubble surface and acoustic radiation emitted by oscillating bubble will be studied. Finally, the current model that is represented by coupled heat equations for bubble's interior and exterior will be compared to uncoupled conventional models.

6.1. Temperature inside and outside the bubble

Temperature distribution obtained through the coupling of the heat equations inside and outside the bubble is going to be studied in the following section. For this purpose, it is necessary to solve Gilmore-Akulichev-Zener model Eqs. (1)–(5) coupled with the equations for the inside temperature Eqs. (6)–(8) and outside temperature Eq. (15). Fig. 5 shows that a vast increase of temperatures inside and outside the

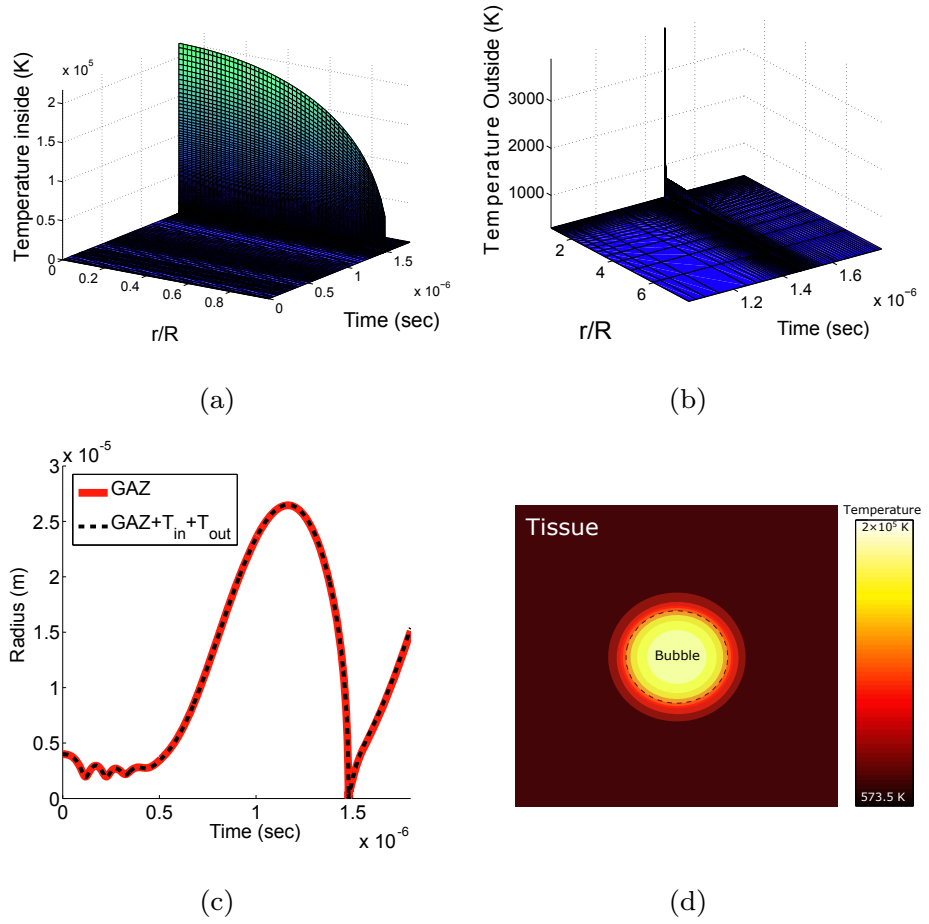

Fig. 5. Temperature distribution during HIFU therapy, $A = 6 * 10^6$ Pa, $R_0 = 4 * 10^{-6}$ m. a) Spatial and temporal distributions of the temperature inside the bubble. b) Spatial and temporal distributions of the temperature outside the bubble. c) Corresponding bubble dynamics for the Gilmore-Akulichev-Zener model and the Gilmore-Akulichev-Zener model coupled with inside and outside temperature models. d) Spatial distribution of the temperature field.

bubble can be observed at the collapsing moment (this pattern can be found in earlier studies [24–27]). The temperature inside the bubble increases due to the dramatic and quick decrease of the bubble volume, whereas the outside temperature rises due to the flux through the interface. The maximum of the inside temperature is located at the bubble center and decreases from it to the interface (that goes in accordance with [15,36]). Owing to the usage of high amplitudes and high frequencies, during HIFU therapy the peak temperature inside the bubble can attain the order of 10^5 K (Fig 5a). This result exhibits an agreement with that in [13], whereas with lower amplitudes and frequencies of the driving pulse, temperature inside the bubble has the order of 10^4 K as it has been shown in [14,25,49,17].

The temperature close to the interface outside the bubble, owing to the temperature continuity, still has a very high value and achieves the order of 10^3 K (Fig. 5b). This high temperature outside the bubble can be obtained only for high amplitude case corresponding to the HIFU driving pulse. While not shown, a noticeable increase of the temperature outside the bubble (i.e. more than 1 K) can be observed within a distance of $100 * R(t)$ from the bubble wall at the collapsing phase (for the currently defined parameters). In fact, elevation of the temperature in tissue due to the cavitation can be seen within a sphere approximately equal to the maximum bubble's size: around 10^{-5} m (in what follows, we define it to be a bubble impact sphere). These high values of the tissue temperature close to the bubble and the existence of the bubble impact sphere emphasize the importance of taking the cavitation into consideration during the simulation of HIFU treatment process.

An increase of the amplitude of the driving pulse raises the bubble's oscillations and boosts values of the temperatures inside and outside the bubble at the collapsing moment. Initially smaller bubbles (starting from 0.1 μm), exposed to the high amplitudes of the ultrasound pressure, tend to generate higher temperatures.

In Fig. 5c, it can be seen that coupling of Gilmore-Akulichev-Zener model with internal and external temperature models does not affect bubble dynamics during the first period of wave propagation. If more periods of bubble oscillations are considered, coupling with temperature models will display difference in bubble dynamics. Traditionally, in Gilmore-Akulichev-Zener model, the pressure inside the bubble is calculated using adiabatic equation of state. In this case, the pressure inside the bubble does not depend on the inside temperature explicitly (only the first term on the right-hand side of Eq. (8) is taken into account). Coupling of the Gilmore-Akulichev-Zener model with the heat equation inside the bubble will lead to the dependency of the pressure on the internal temperature (the second term on the right-hand side of Eq. (8)). However, it is also necessary to consider the dependency of the pressure inside the bubble on the vapor mass flux through the bubble wall [Eqs. (9)–(14)]. In the subsection 6.4, it will be shown that bubble dynamics are affected by coupling of Gilmore-Akulichev-Zener model with heat equations, when several periods of bubble oscillations are considered (Fig. 11a).

6.2. Contribution of the cavitation heat sources

In the current section, the influence of cavitation heat sources

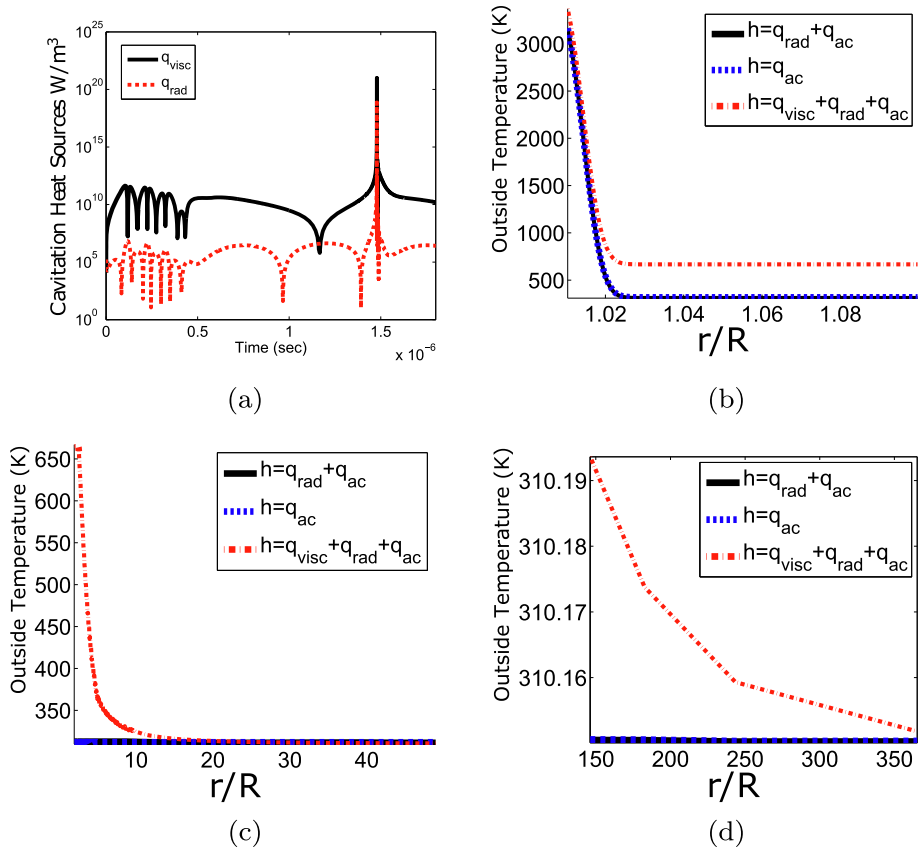

Fig. 6. Contribution of the cavitation heat sources to the temperature elevation for one bubble collapse based on the results obtained by taking into account only the acoustic heat source q_{ac}; acoustic heat source q_{ac} and radiation cavitation heat source q_{rad}; acoustic heat source q_{ac}, radiation cavitation heat source q_{rad} and viscous cavitation heat source q_{visc}. $A = 6 * 10^6$ Pa, $R_0 = 4 * 10^{-6}$ m, $r_{visc} = 5{\cdot}R(t)$, $r_{rad} = 20{\cdot}R(t)$. a) Comparison of the cavitation heat sources. b) Temperature outside the bubble at the collapsing moment close to the bubble wall ($1R(t) \leqslant r \leqslant 1.1R(t)$). c) Temperature outside the bubble at the collapsing moment farther from the bubble wall ($2R(t) \leqslant r \leqslant 50R(t)$). d) Temperature outside the bubble at the collapsing moment far from bubble wall ($150R(t) \leqslant r \leqslant 350R(t)$).

(viscous source q_{visc} and radiation heat source q_{rad} in bioheat Eq. (15)) on the temperature elevation in tissue will be investigated. Viscous heat source q_{visc} arises from a work of viscous friction forces acting on the surface of the oscillating bubble. Radiation heat source q_{rad} is caused by the emission of a sound wave by bubble's radial pulsations.

It should be noted that in the current study, the radii r_{visc} and r_{rad} of the spheres, upon which the energy is distributed, have to be chosen. In the literature, different approaches of calculation of these parameters have been used [20,18,6,19,23,22]. In the current study, we are following the method described in [20,18] by choosing the certain radii of shell spheres, upon which the viscous and radiation energies are absorbed. The currently used values of r_{visc} and r_{rad} are estimated from the consideration of values of spheres' radii in [20,18] (which are of the order of the magnitude 10^{-4} m) and the value corresponding to the maximum radius of the bubble that has been observed in the present simulations. As it can be seen in Eq. (16) and Eq. (18), the decrease of the values of r_{visc} and r_{rad} will result in an increase of the temperature values. Namely, the decrease of the currently used $r_{visc} = 5R$ to $2R$ results in the increase of the temperature close to the bubble interface by 10 times. In the future, if the experimental data are available, the currently used values of r_{visc} and r_{rad} should be corrected accordingly.

Both cavitation heat sources reflect the bubble dynamics precisely: their peaks might be observed at the bubble collapsing phase (Fig. 6a). The behavior of cavitation heat sources does not depend on the choice of values of r_{visc} and r_{rad}. It is prescribed by the bubble's radial motion, i.e. by $R(t)$, dR/dt and d^2R/dt^2.

Fig. 6b, c, d shows the spatial distribution of the temperature outside the bubble at the collapsing moment. It can be seen that cavitation heat sources can not be treated as the main mechanisms responsible for the elevation of the temperature outside the bubble (rapid decrease of the volume of the bubble leads to a large increase of the temperature inside the bubble, which also results in a high temperature close to the bubble wall). However, they might make some contribution to the increase of the temperature. The viscous cavitation heat source q_{visc} leads to the temperature elevation at the collapsing moment outside the bubble, especially close to the bubble wall, as shown in Fig. 6. In contrast, the radiation cavitation heat source q_{rad} does not yield significant influence on the temperature if only one collapse of the bubble is simulated. Impact of the radiation cavitation heat source on the temperature elevation and bubble dynamics can be observed only if a longer time is considered. Therefore, since both cavitation heat sources contribute to the temperature elevation, they should be kept in the formulation in future studies.

6.3. Elasticity and relaxation time effects

Most of the previous studies investigated bubble dynamics and temperature elevation in a Newtonian fluid. For the soft tissue, it is important to take into account the viscoelastic nature of the medium. In the following section, the influence of soft tissue's viscoelastic properties on the temperature distribution associated with a cavitation presence will be investigated.

In agreement with earlier investigations [29,50,42], increase in elasticity modulus G results in a dramatic restriction of the bubble oscillations and their amplitude (Fig. 7a). For the current simulations, the range of elasticity values for tissue was set accordingly to [51,52,42,30]: 0–10 MPa. The diminution of bubble oscillations is associated with the decrease of both temperatures inside and outside the

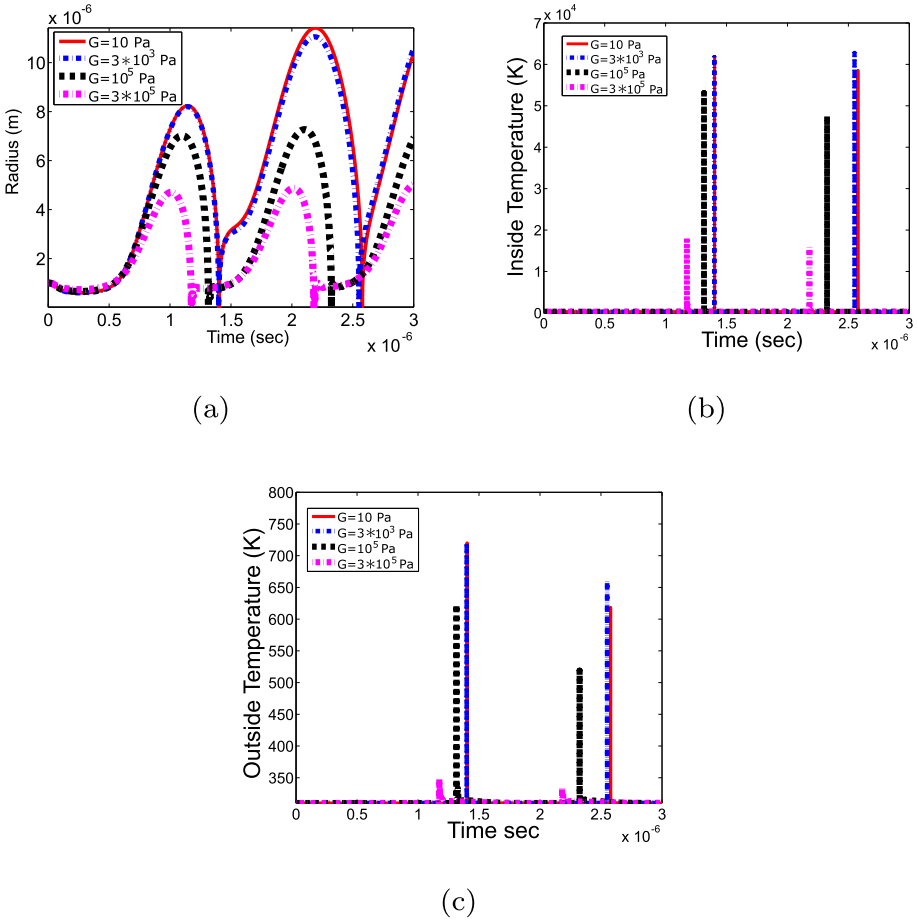

Fig. 7. Soft tissue's elasticity modulus G effect for the Gilmore-Akulichev-Zener model coupled with temperature models. $A = 1 * 10^6$ Pa, $R_0 = 1 * 10^{-6}$ m. a) Bubble dynamics. b) Temperature inside the bubble at the middle of the bubble radius. c) Temperature outside the bubble at $r/R(t) = 13$.

bubble (Fig. 7b, c). However, due to the growing behavior of the bubble mentioned in subsection 6.1, the elasticity effect can become less prominent during several bubble collapses.

Relaxation time effect on bubble dynamics strongly depends on the period of ultrasound wave (Fig. 8, [29]). At low values of the relaxation time, when λ is much smaller than the period of the ultrasound wave (for example, $\lambda = 10^{-9}$ s), there is almost no difference with a case of $\lambda = 0$ s in terms of bubble oscillations. When relaxation time is close to the period of the ultrasound wave ($10^{-7}\,\text{s} \leqslant \lambda < 10^{-6}$ s), the frequency of bubble oscillations diminishes and their amplitude increases. With λ being approximately equal to the period of the wave ($\lambda = 10^{-6}$ s), the amplitude of the oscillations reaches the maximum value. With a further increase of the relaxation time, the amplitude of bubble oscillations starts decreasing. Relaxation time effect on the temperature values resembles its impact on the bubble radius. When relaxation time is approximately equal to the period of the ultrasound wave, values of temperatures inside and outside the bubble at the collapsing moment are the highest ones (Fig. 8b, c). However, collapse itself will take place more rarely. When relaxation time values are bigger or smaller than the period of the ultrasound wave, the temperature at the collapsing moment is smaller, but collapse itself can be observed much more frequently. Thus, the relaxation time effect on the temperature distribution resembles its impact on the bubble dynamics and, hence, strongly depends on the period of the driving pulse. However, it should be mentioned that since elasticity can suppress oscillations, larger elasticity values make bubble behavior more chaotic with respect to the relaxation time variation, so the impact of relaxation time on the temperature distribution also can be less pronounced.

6.4. *Effect of the vapor mass flux*

In order to examine the significance of vapor mass flux, the simulations have been performed with and without consideration of the diffusion model. By the definition of the applied diffusion model, mass flux of vapor per unit area across the interface $\dot{m}_v''$ is negative for the flow in the direction to the exterior of the bubble [36]. At the collapsing moment, vapor mass flux $\dot{m}_v''$ is negative (Fig. 9d), therefore, vapor emission takes place. Except at the collapsing moment, vapor mass flux $\dot{m}_v''$ is very small, but positive, which corresponds to the flow of vapor into the bubble. Vapor mass concentration C inside the bubble attains the highest value when the bubble's size reaches its maximum (Fig. 9c, this result goes in accordance with [36]). In the bubble growth phase, the value of the vapor mass concentration C reaches its highest value at the bubble wall and decreases towards the bubble center. At the collapsing moment, vapor concentration dramatically decreases (Fig. 9c), because vapor transfer to the exterior of the bubble takes place. For the same reason, the situation with a spatial distribution of the vapor mass concentration changes: now, the smallest value of C is obtained at the bubble wall and then it monotonically increases to the bubble center.

Temperatures inside and outside the bubble with vapor mass flux are smaller than those without consideration of vapor (Figs. 9b, 10). This happens because, in the case of taking into account vapor mass flux, bubble size at the collapsing moment is bigger than that without vapor effect. It is linked to the rectified diffusion growth effect when a shift of effective initial radius of the bubble takes place. With the increase of effective radius, bubble size enlarges with time. Such an enlargement of the bubble size associated with the rectified diffusion can be easily seen in long time simulations (Fig. 11). Therefore, because of

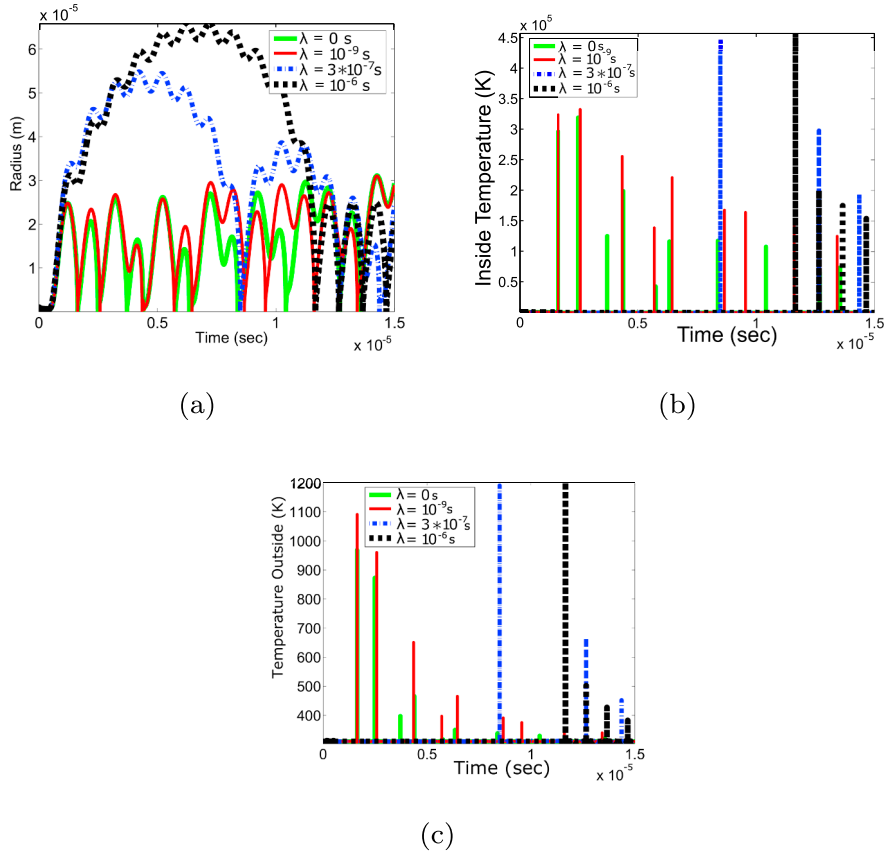

Fig. 8. Soft tissue's relaxation time λ effect for the Gilmore-Akulichev-Zener model coupled with temperature models. $A = 5 * 10^6$ Pa, $R_0 = 1 * 10^{-6}$ m, $G = 3 * 10^3$ Pa, $\mu = 0.02$ Pa·s. a) Bubble dynamics. b) Temperature inside the bubble at the middle of the bubble radius. c) Temperature outside the bubble at $r/R(t) = 13$.

the bigger bubble size at the collapsing moment, rectified diffusion growth effect results in lower temperatures inside and outside the bubble. The difference in temperatures obtained with and without vapor mass flux decreases from the bubble wall to the infinity. Close to the bubble wall ($3 \leqslant r/R \leqslant 7$), the outside temperature in tissue can be 1.5 times smaller, when vapor mass flux is taken into account (Fig. 10a). Whereas far from the bubble wall ($100 \leqslant r/R \leqslant 200$) the difference is less than 1 °C.

All in all, it can be concluded that vapor mass flux is important in terms of the temperature outside the bubble. Compared to the case of not taking it into account, the outside temperature at the bubble wall can be smaller by a factor of 1.5 times.

6.5. Comparison with separate temperature models of bubble's interior and exterior

In order to highlight the significance of the current coupling model, temperature distribution obtained by Gilmore-Akulichev-Zener model coupled with two temperature models (and diffusion model) Eqs. (24)–(32) was compared to that obtained by the models without consideration of coupling.

In most of the previous studies, calculation of the temperature within the bubble was performed with the outside temperature being unperturbed [10–16]. The analysis below is aimed to reveal if there is a difference, in terms of the temperatures inside the bubble, between the conventional approach of its calculation and the case when the temperature outside the bubble does not remain constant anymore (i.e. with the current model that simulates outside temperature as a function of space and time and assumes interrelation of the temperatures inside and outside the bubble). The current coupled model without and with vapor diffusion is denoted as $M1$ and $M2$, respectively. The comparison was made between the current model results and a solution obtained by Gilmore-Akulichev-Zener model that is coupled with the inside temperature model only Eqs.)(1)–(5), Eqs. (6)–(8) (or with inside temperature model with incorporated diffusion model into it Eqs. (9)–(14)). In Gilmore-Akulichev-Zener model coupled with inside temperature model only, the outside temperature was assumed to be constant (so $T_{out} = const = T_\infty$). These internal models without and with vapor diffusion are denoted as $M3$ and $M4$, respectively. From Fig. 12 it can be concluded that the temperature inside the bubble can be described precisely even by uncoupled models.

However, during the treatment, there is an interest in the elevation of the temperature in tissue outside the bubble as well. Originally, in order to calculate the temperature in the bubble surrounding medium, only one bioheat equation was employed that was solved separately from the inside temperature model [18–23]. The bubble was incorporated into the bioheat equation by time-averaged cavitation heat sources [18]. With an objective to see if there is any significance in coupling the bioheat equation with the inside temperature equations, the currently proposed model was compared to the solution of the bioheat equation for tissue heating not coupled with other models [Eq. (15)]. Cavitation heat sources [Eqs. (16), (18)] in the bioheat equation were calculated on the base of Gilmore-Akulichev-Zener equation that was solved separately beforehand. This model will be referred as $M5$.

Fig. 13 shows values of the temperature at the bubble wall at the collapsing moment for all five above-mentioned models. Fig. 13 reveals that the non-coupled internal models overestimate the interface temperature at the collapsing moment compared to the models, in which bubble's interior and exterior are interrelated. The non-coupled external model ($M5$) underestimates the collapse temperature at the bubble wall. Therefore, the interface temperature in the coupled models is a reasonable interpolation between those in the non-coupled internal

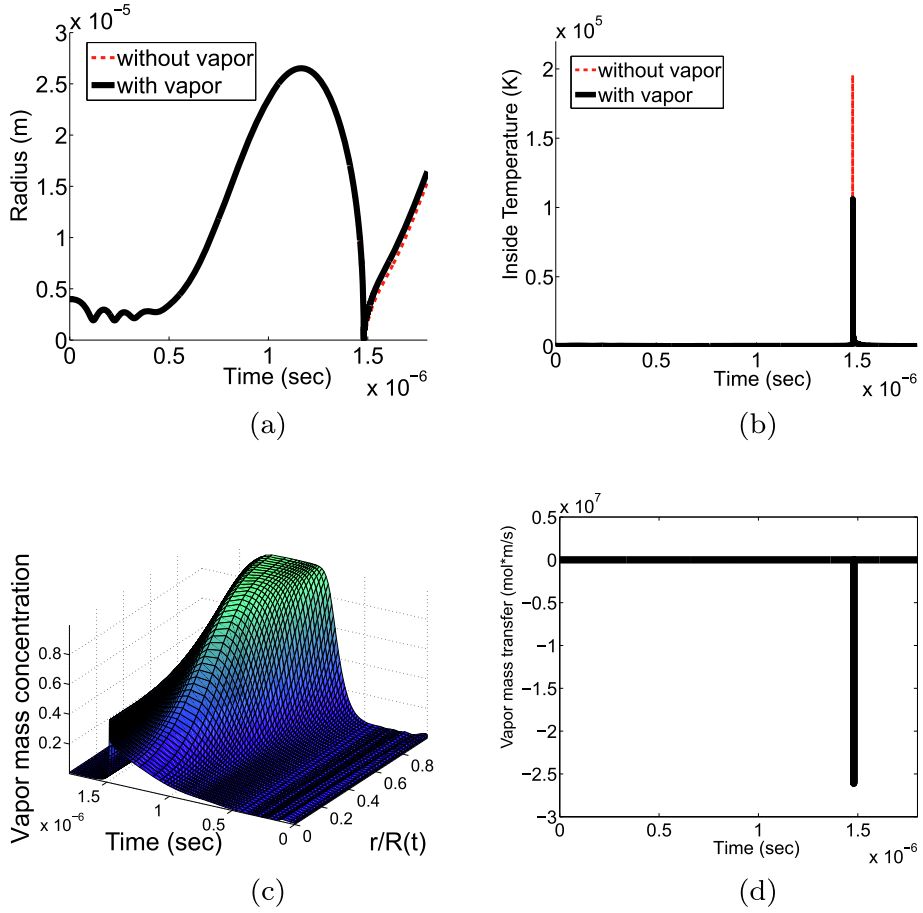

Fig. 9. Effect of the vapor mass flux. $A = 6 * 10^6$ Pa, $R_0 = 4 * 10^{-6}$ m. a) Bubble dynamics. b) Temperature inside the bubble at the middle of the bubble radius. c) Spatial and temporal distributions of vapor mass concentration C. d) Vapor mass flux through the bubble wall $\dot{m}_v''$.

and external models.

Fig. 14 compares the models in terms of the outside temperature distribution. The temporal dynamics of the outside temperature for all coupled and non-coupled models display an increase of the temperature at the collapsing moment. However, there is a difference between the models in the value of the collapse temperature. Fig. 14 shows that the increase of the temperature outside the bubble can not be described precisely by the solution of the non-coupled external model. The assumption of continuity of the temperature distribution inside and outside the bubble and the equality of fluxes through the bubble wall are important conditions and show the significant increase in the temperature outside the bubble. The solution obtained without taking the coupling effect into consideration shows a raise of the tissue temperature in less than one degree due to the presence of cavitation, whereas solutions obtained by coupled model show that the temperature at the bubble-tissue interface takes the order of 10^3 K. Hence, it can be concluded that coupling is essential in order to take into account the temperature elevation associated with bubble oscillations.

However, it should be noted that the current coupled model is a good choice in terms of the solution quality and computational time if the simulation time is within the order of magnitude of around 10^{-5} s. If the objective is to simulate the temperature distribution after several seconds of the treatment, the computational time of the current model will be too long. The only remedy, in this case, would be to use the non-coupled heat equation. From the current research, it can be seen that even though there is a vast increase of the temperatures at the collapsing moment, the temperature outside the bubble does not increase further in space than approximately the maximum radius of the bubble

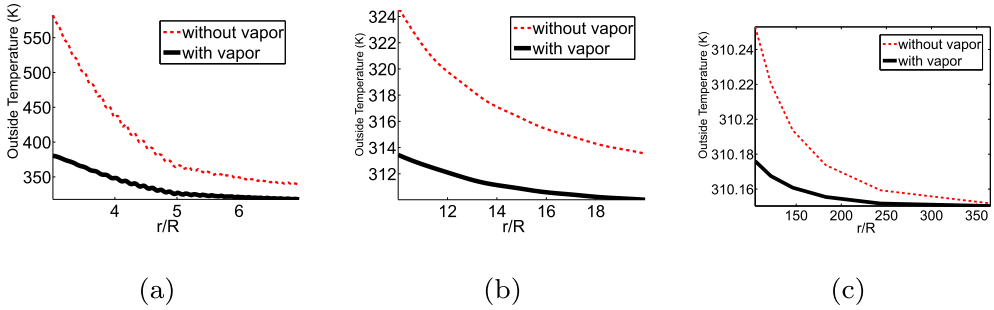

Fig. 10. Effect of the vapor mass flux on the temperature outside the bubble. $A = 6 * 10^6$ Pa, $R_0 = 4 * 10^{-6}$ m. a) Temperature outside the bubble at the collapsing moment close to the bubble wall ($3R(t) \leqslant r \leqslant 7R(t)$). b) Temperature outside the bubble at the collapsing moment farther from the bubble wall ($10R(t) \leqslant r \leqslant 20R(t)$). c) Temperature outside the bubble at the collapsing moment far from bubble wall ($100R(t) \leqslant r \leqslant 350R(t)$).

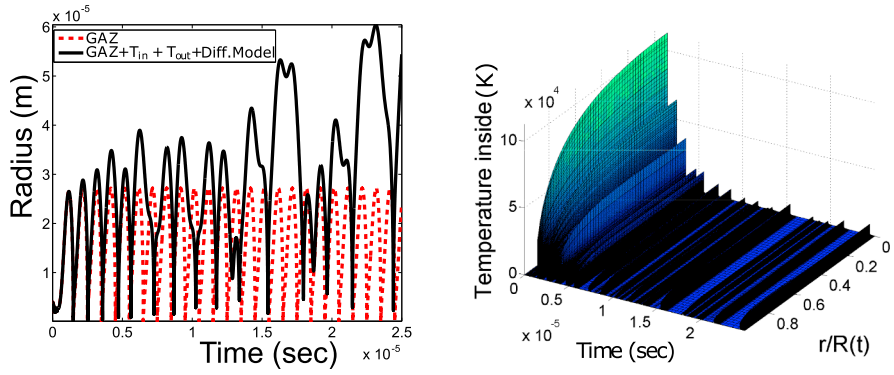

(a) (b)

Fig. 11. Rectified diffusion growth effect for long time simulations. $A = 6 * 10^6$ Pa, $R_0 = 4 * 10^{-6}$ m. a) Bubble dynamics. b) Spatial and temporal distributions of the temperature inside the bubble.

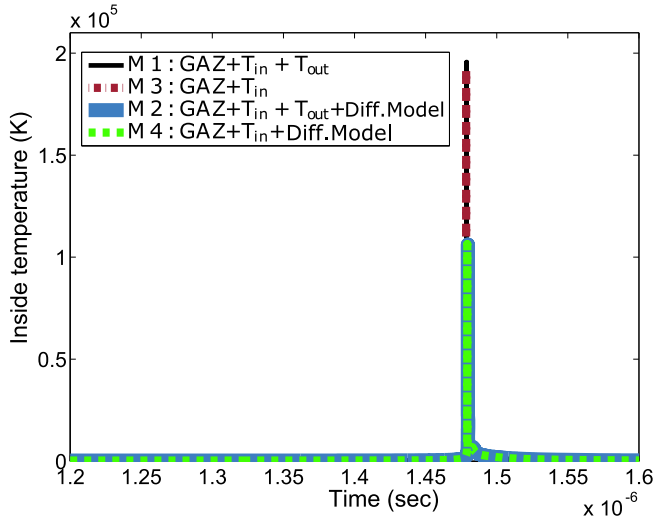

Fig. 12. Comparison of the predicted temperature distributions inside the bubble obtained by different models. $A = 6 * 10^6$ Pa, $R_0 = 4 * 10^{-6}$ m. Temperature inside the bubble at the middle of the bubble radius ($r = \frac{R(t)}{2}$) with the usage of four different models: $M1$, $M2$ – coupled temperature models without and with vapor diffusion; $M3$, $M4$ – internal temperature models without and with vapor diffusion.

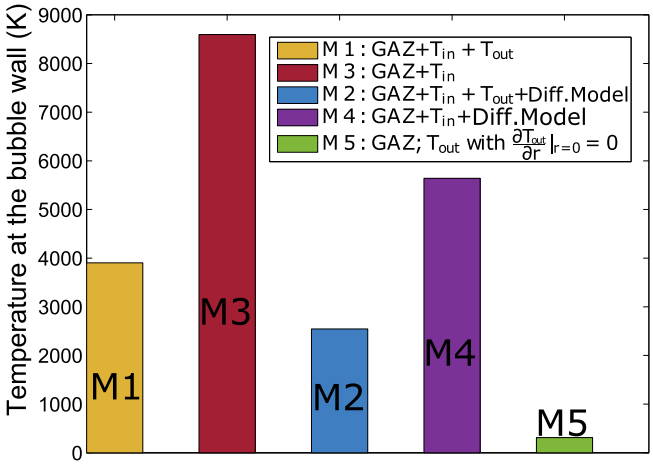

Fig. 13. Comparison of the predicted temperatures at the bubble wall at the collapsing moment ($t = 1.48 \cdot 10^{-6}$ s) by different models. $A = 6 * 10^6$ Pa, $R_0 = 4 * 10^{-6}$ m. The following models were used: $M1$, $M2$ – the coupled temperature models without ($M1$) and with ($M2$) vapor diffusion; $M3$, $M4$ – the internal temperature models without ($M3$) and with ($M4$) vapor diffusion; $M5$ – the external temperature model.

(subsection 6.1). Also, during the simulation time around 10^{-5} s, the noticeable elevation of the post-collapse temperature can not be observed. The hypothesis can be made that only the work of the cavitation heat sources over several seconds might increase significantly the tissue temperature. Thereby, the non-coupled heat equation, which simulates several seconds of the cavitation enhanced elevation of the temperature, should incorporate the cavitation heat sources. Those cavitation heat sources should be obtained on a base of the current coupled model and time-averaged over several pulse periods. For the simulation of the temperature after several seconds of the treatment, the future investigations and comparison with experiments are required.

7. Conclusions

Due to the emergence of biomedical applications, the analysis of the temperature distribution associated with bubble oscillations in soft tissue has become important. In most of the previous studies, only one heat equation was considered in order to simulate either bubble's interior or exterior. In the current study, the heat equations inside and outside the bubble are interrelated.

The Gilmore-Akulichev-Zener model coupled with two heat equations for the description of temperatures inside and outside the bubble has been proposed. This model is suitable for the simulation of the bubble dynamics and the corresponding temperature distribution in soft tissue that is a subject to HIFU pulse wave. The current model is also coupled with the diffusion model for the calculation of the vapor mass concentration inside the bubble and the vapor mass flux through the bubble wall.

As it was anticipated, temperature elevation reflects bubble dynamics. In the sense that during a dramatic bubble collapse, temperatures inside and outside the bubble increase significantly. In the case of a single HIFU pulse, the temperature inside the bubble reaches the order of 10^5 K, whereas tissue temperature close to the bubble wall can be heated up to 10^3 K. In terms of the distance, temperature elevation in tissue at the collapsing moment can be observed within a sphere approximately equal to the maximum size reached by bubble during its oscillations: around 10^{-5} m. This fact emphasizes that the presence of cavitation can not be ignored. It can cause an incomparably higher temperature in soft tissue.

For the temperature outside the bubble, it was expected that consideration of cavitation heat sources will result in a dramatic increase of the temperature outside the bubble compared to the case of taking into account only acoustic heating of media. However, the main heating

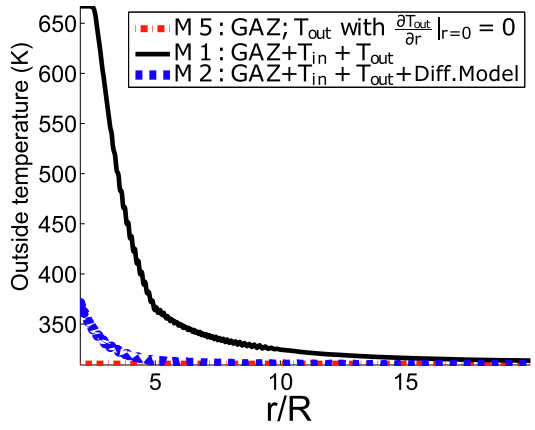

(a)

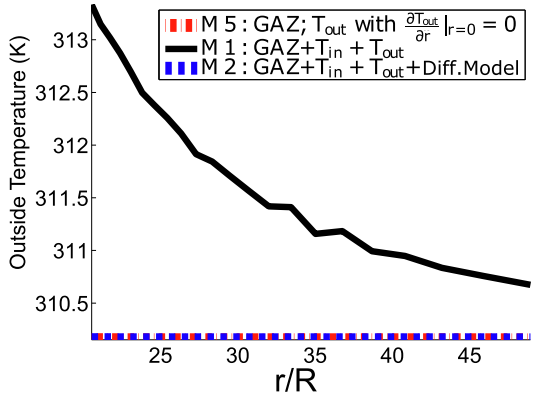

(b)

Fig. 14. Comparison of the temperature distributions outside the bubble obtained by different models. $A = 6 * 10^6$ Pa, $R_0 = 4 * 10^{-6}$ m. The initial temperature in the medium was 310.15 K. Temperature outside the bubble at the collapsing moment ($t = 1.48 \cdot 10^{-6}$ s) obtained by three different models: $M1$, $M2$ – the coupled temperature models without and with vapor diffusion; $M5$ – the external temperature model. a) The predicted temperature outside the bubble close to the bubble wall ($2R(t) \leqslant r \leqslant 20R(t)$). b) The predicted temperature outside the bubble farther from the bubble wall ($20R(t) \leqslant r \leqslant 50R(t)$).

mechanism responsible for the elevation of the temperature outside the bubble during a few microseconds is the bubble collapse itself (that entails a significant increase of the temperature inside the bubble). Viscous cavitation heat source increases the tissue temperature, especially close to the bubble wall. Impact of radiation cavitation heat source can be observed in a longer time calculation. Therefore, in future studies, cavitation heat sources should not be omitted in mathematical models.

The influence of soft tissue's viscoelastic properties on the temperature distribution has been investigated. Since bubble oscillations are damped by the increase in elasticity of the surrounding medium [29,50,42] the values of temperatures inside and outside the bubble decrease as well. The relaxation time effect for the temperature distribution also clearly corresponds to the dependency of bubble dynamics on the relaxation time and, thus, strongly depends on the period of the ultrasound wave.

Simulation results that take into account the vapor mass flux displayed the rectified growth effect. It consists of the bubble's larger size with time and is related to the mass diffusion through the interface. Particularly, bubble's bigger size at the collapsing phase results in smaller temperatures inside and outside the bubble compared to those without vapor mass flux. When vapor mass flux is taken into account, the outside temperature in tissue can be up to 1.5 times smaller. Therefore, the vapor mass flux has an impact on the temperature distribution.

The comparison of the temperature distribution obtained from the current model with the ones obtained by solving the equations for bubble's interior and exterior separately was performed. It was shown that coupling approach is critically important in terms of the temperature outside the bubble. If the non-coupled heat equation outside the bubble is solved, the temperature increase is less than one degree at the collapsing moment. Whilst application of the coupled model raises the temperature close to the bubble wall that is of the order of 10^3 K. Nevertheless, both coupled and uncoupled models showed the same values of the temperature inside the bubble. Therefore, the temperature inside the bubble can be calculated precisely without coupling with the exterior of the bubble.

Now, we are planning to extend the current approach to model multiple bubbles and include the bubble-bubble interaction. Also, the time scale is planned to be expanded to a few seconds instead of microseconds. This expansion might change the significance of the current heating mechanisms on the tissue. Then, the model is going to be compared with experiments for tissue heating with cavitation presence in HIFU therapy [7].

Acknowledgements

We would like to thank professor Marc Thiriet for the discussion on histological structure of soft tissue. This research was supported by the Ministry of Science and Technology, R.O.C., under the grant MOST-106-2115-M-400-001 and by National Health Research Institute's project BN-107-PP-08.

References

[1] Y.-F. Zhou, High intensity focused ultrasound in clinical tumor ablation, World J. Clin. Oncol. 2 (2011) 8.
[2] M. Solovchuk, T.W. Sheu, M. Thiriet, Simulation of nonlinear Westervelt equation for the investigation of acoustic streaming and nonlinear propagation effects, J. Acoust. Soc. Am. 134 (2013) 3931–3942.
[3] M.A. Solovchuk, M. Thiriet, T.W. Sheu, Computational study of acoustic streaming and heating during acoustic hemostasis, Appl. Therm. Eng. (2017).
[4] O. Al-Bataineh, J. Jenne, P. Huber, Clinical and future applications of high intensity focused ultrasound in cancer, Cancer Treat. Rev. 38 (2012) 346–353.
[5] T. Leslie, J. Kennedy, High intensity focused ultrasound in the treatment of abdominal and gynaecological diseases, Int. J. Hyperth. 23 (2007) 173–182.
[6] C.C. Coussios, R.A. Roy, Applications of acoustics and cavitation to noninvasive therapy and drug delivery, Annu. Rev. Fluid Mech. 40 (2008) 395–420.
[7] M.A. Solovchuk, S.C. Hwang, H. Chang, M. Thiriet, T.W. Sheu, Temperature elevation by hifu in ex vivo porcine muscle: Mri measurement and simulation study, Med. Phys. 41 (2014).
[8] C.A. Damianou, K. Hynynen, X. Fan, Evaluation of accuracy of a theoretical model for predicting the necrosed tissue volume during focused ultrasound surgery, IEEE Trans. Ultrason. Ferroelectr. Freq. Control 42 (1995) 182–187.
[9] V. Sorrentino, Experimental evaluation of a simple field equation model for prediction of temperature distribution in focused ultrasound surgery (Ph.D. thesis), Boston University, 1998.
[10] R. Löfstedt, B.P. Barber, S.J. Putterman, Toward a hydrodynamic theory of sonoluminescence, Phys. Fluids A 5 (1993) 2911–2928.
[11] B.P. Barber, R.A. Hiller, R. Löfstedt, S.J. Putterman, K.R. Weninger, Defining the unknowns of sonoluminescence, Phys. Rep. 281 (1997) 65–143.
[12] A. Prosperetti, Thermal effects and damping mechanisms in the forced radial oscillations of gas bubbles in liquids, J. Acoust. Soc. Am. 61 (1977) 17–27.
[13] M.P. Brenner, S. Hilgenfeldt, D. Lohse, Single-bubble sonoluminescence, Rev. Mod. Phys. 74 (2002) 425.
[14] S. Hilgenfeldt, S. Grossmann, D. Lohse, Sonoluminescence light emission, Phys. Fluids 11 (1999) 1318–1330.
[15] A. Prosperetti, L.A. Crum, K.W. Commander, Nonlinear bubble dynamics, J. Acoust. Soc. Am. 83 (1988) 502–514.
[16] A. Prosperetti, The thermal behaviour of oscillating gas bubbles, J. Fluid Mech. 222 (1991) 587–616.
[17] S. Merouani, O. Hamdaoui, Y. Rezgui, M. Guemini, Theoretical estimation of the temperature and pressure within collapsing acoustical bubbles, Ultrason. Sonochem. 21 (2014) 53–59.
[18] C.H. Farny, R.G. Holt, R.A. Roy, The correlation between bubble-enhanced hifu heating and cavitation power, IEEE Trans. Biomed. Eng. 57 (2010) 175–184.

[19] S. Hilgenfeldt, D. Lohse, The acoustics of diagnostic microbubbles: dissipative effects and heat deposition, Ultrasonics 38 (2000) 99–104.
[20] F. Chavrier, J. Chapelon, A. Gelet, D. Cathignol, Modeling of high-intensity focused ultrasound-induced lesions in the presence of cavitation bubbles, J. Acoust. Soc. Am. 108 (2000) 432–440.
[21] C. Coussios, C. Farny, G. Ter Haar, R. Roy, Role of acoustic cavitation in the delivery and monitoring of cancer treatment by high-intensity focused ultrasound (hifu), Int. J. Hyperth. 23 (2007) 105–120.
[22] S. Hilgenfeldt, D. Lohse, M. Zomack, Sound scattering and localized heat deposition of pulse-driven microbubbles, J. Acoust. Soc. Am. 107 (2000) 3530–3539.
[23] R.G. Holt, R.A. Roy, Measurements of bubble-enhanced heating from focused, mhz-frequency ultrasound in a tissue-mimicking material, Ultrasound Med. Biol. 27 (2001) 1399–1412.
[24] L. Stricker, A. Prosperetti, D. Lohse, Validation of an approximate model for the thermal behavior in acoustically driven bubbles, J. Acoust. Soc. Am. 130 (2011) 3243–3251.
[25] V. Kamath, A. Prosperetti, F. Egolfopoulos, A theoretical study of sonoluminescence, J. Acoust. Soc. Am. 94 (1993) 248–260.
[26] O. Shpak, L. Stricker, M. Versluis, D. Lohse, The role of gas in ultrasonically driven vapor bubble growth, Phys. Med. Biol. 58 (2013) 2523.
[27] C. Barajas, E. Johnsen, The effects of heat and mass diffusion on freely oscillating bubbles in a viscoelastic, tissue-like medium, J. Acoust. Soc. Am. 141 (2017) 908–918.
[28] F.R. Gilmore, The growth or collapse of a spherical bubble in a viscous compressible liquid (1952).
[29] E. Zilonova, M. Solovchuk, T. Sheu, Bubble dynamics in viscoelastic soft tissue in high-intensity focal ultrasound thermal therapy, Ultrason. Sonochem. 40 (2018) 900–911.
[30] C. Hua, E. Johnsen, Nonlinear oscillations following the rayleigh collapse of a gas bubble in a linear viscoelastic (tissue-like) medium, Phys. Fluids 25 (2013) 083101 .
[31] H.H. Pennes, Analysis of tissue and arterial blood temperatures in the resting human forearm, J. Appl. Physiol. 1 (1948) 93–122.
[32] W. Wulff, The energy conservation equation for living tissue, IEEE Trans. Biomed. Eng. (1974) 494–495.
[33] M.M. Chen, K.R. Holmes, Microvascular contributions in tissue heat transfer, Ann. N. Y. Acad. Sci. 335 (1980) 137–150.
[34] Y. Xuan, W. Roetzel, Bioheat equation of the human thermal system, Chem. Eng. Technol. 20 (1997) 268–276.
[35] A. Nakayama, F. Kuwahara, A general bioheat transfer model based on the theory of porous media, Int. J. Heat Mass Transfer 51 (2008) 3190–3199.
[36] A.T. Preston, Modeling heat and mass transfer in bubbly cavitating flows and shock waves in cavitating nozzles (Ph.D. thesis), California Institute of Technology, 2004.
[37] X. Yang, R.A. Roy, R.G. Holt, Bubble dynamics and size distributions during focused ultrasound insonation, J. Acoust. Soc. Am. 116 (2004) 3423–3431.
[38] R. Milo, P. Jorgensen, U. Moran, G.M. Weber, M. Springer, Bionumbers – the database of key numbers in molecular and cell biology, Nucleic Acids Res. 38 (2010) 750–753.
[39] E.P. Widmaier, H. Raff, K.T. Strang, Vander's Human Physiology, Print, 2015.
[40] D.H. Cormack, A.W. Ham, Ham's Histology, Lippincott, New York, 1987.
[41] M.A. Swartz, M.E. Fleury, Interstitial flow and its effects in soft tissues, Annu. Rev. Biomed. Eng. 9 (2007) 229–256.
[42] X. Yang, C.C. Church, A model for the dynamics of gas bubbles in soft tissue, J. Acoust. Soc. Am. 118 (2005) 3595–3606.
[43] C.R. Leeson, T.S. Leeson, A.A. Paparo, Textbook of Histology, WB Saunders Company, 1985.
[44] F.A. Duck, Physical Properties of Tissues: A Comprehensive Reference Book, Academic Press, 2013.
[45] M.A. Solovchuk, T.W. Sheu, M. Thiriet, W.-L. Lin, On a computational study for investigating acoustic streaming and heating during focused ultrasound ablation of liver tumor, Appl. Therm. Eng. 56 (2013) 62–76.
[46] M. Solovchuk, T.W.-H. Sheu, M. Thiriet, Multiphysics modeling of liver tumor ablation by high intensity focused ultrasound, Commun. Comput. Phys. 18 (2015) 1050–1071.
[47] M.A. Diaz, M.A. Solovchuk, T.W. Sheu, A conservative numerical scheme for modeling nonlinear acoustic propagations in thermoviscous homogeneous media, J. Comput. Phys. (2018).
[48] D.R. Lide, et al., CRC Handbook of Chemistry and Physics (1947) 12J204.
[49] D.F. Gaitan, L.A. Crum, C.C. Church, R.A. Roy, Sonoluminescence and bubble dynamics for a single, stable, cavitation bubble, J. Acoust. Soc. Am. 91 (1992) 3166–3183.
[50] C.C. Church, X. Yang, The mechanical index and cavitation in tissue, J. Acoust. Soc. Am. 117 (2005) 2530–2530.
[51] E.L. Madsen, H.J. Sathoff, J.A. Zagzebski, Ultrasonic shear wave properties of soft tissues and tissuelike materials, J. Acoust. Soc. Am. 74 (1983) 1346–1355.
[52] P.N. Wells, H.-D. Liang, Medical ultrasound: imaging of soft tissue strain and elasticity, J. R. Soc. Interface 8 (2011) 1521–1549.
[53] E. Vlaisavljevich, K.-W. Lin, A. Maxwell, M.T. Warnez, L. Mancia, R. Singh, A.J. Putnam, B. Fowlkes, E. Johnsen, C. Cain, et al., Effects of ultrasound frequency and tissue stiffness on the histotripsy intrinsic threshold for cavitation, Ultrasound Med. Biol. 41 (2015) 1651–1667.
[54] M. Warnez, E. Johnsen, Numerical modeling of bubble dynamics in viscoelastic media with relaxation, Phys. Fluids 27 (2015) 063103 .
[55] J.M. Wallace, P.V. Hobbs, Atmospheric Science: An Introductory Survey vol. 92, Elsevier, 2006.